Review

Characteristics of atmospheric gravity waves observed using the MU (Middle and Upper atmosphere) radar and GPS (Global Positioning System) radio occultation

By Toshitaka TSUDA[*1,†]

(Communicated by Atsuhiro NISHIDA, M.J.A.)

Abstract: The wind velocity and temperature profiles observed in the middle atmosphere (altitude: 10–100 km) show perturbations resulting from superposition of various atmospheric waves, including atmospheric gravity waves. Atmospheric gravity waves are known to play an important role in determining the general circulation in the middle atmosphere by dynamical stresses caused by gravity wave breaking. In this paper, we summarize the characteristics of atmospheric gravity waves observed using the middle and upper atmosphere (MU) radar in Japan, as well as novel satellite data obtained from global positioning system radio occultation (GPS RO) measurements. In particular, we focus on the behavior of gravity waves in the mesosphere (50–90 km), where considerable gravity wave attenuation occurs. We also report on the global distribution of gravity wave activity in the stratosphere (10–50 km), highlighting various excitation mechanisms such as orographic effects, convection in the tropics, meteorological disturbances, the subtropical jet and the polar night jet.

Keywords: atmospheric gravity wave, middle atmosphere, wave breaking, saturated spectrum, the MU radar, GPS radio occultation

1. Introduction

The main forces at work in the atmosphere are the Coriolis force, the pressure gradient force and gravity. Above the planetary boundary layer, the atmospheric column is generally stably stratified. Therefore, gravity acts as a restoring force against any vertical movement in the atmosphere, causing air cells to oscillate in the vertical, which is the basic mechanism behind atmospheric gravity waves.[1),2)] Atmospheric gravity waves are medium-scale waves with the horizontal wavelength ranging between several tens and several thousands of kilometers and a vertical wavelength of several kilometers. At mid-latitudes, their period varies from several minutes to about one day. Unlike surface waves, atmospheric gravity waves can propagate vertically, and transport momentum and kinetic energy upward. Various investigations into the excitation, propagation, and decay of atmospheric gravity waves have been conducted through ground-based observations and satellite measurements.[3)]

The fundamental structure of Earth's atmosphere is largely controlled by the heating due to solar radiation, which is the highest at the equator and decreases toward the poles. In the middle atmosphere (10–100 km altitude), consisting of the stratosphere (10–50 km), the mesosphere (50–90 km) and a part of the lower thermosphere (90–150 km), the zonal wind velocity can reach magnitudes as large as 80 m/s in mid-latitudes at an altitude of about 50 km. It was expected to remain strong up to an altitude of 100 km based on radiative equilibrium considerations. However, rocketsonde observations from the 1960s reported a major inconsistency in that the mean zonal winds, instead of remaining strong, become weaker or even reverse direction above about an altitude of 70 km.[4),5)] These observations posed an important challenge to the field of atmospheric science in 1970s.[6)] In order to explain this weakening

    [*1] Research Institute for Sustainable Humanosphere (RISH), Kyoto University, Kyoto, Japan.
    [†] Correspondence should be addressed: T. Tsuda, Research Institute for Sustainable Humanosphere (RISH), Kyoto University, Uji, Kyoto 611-0011, Japan (e-mail: tsuda@rish.kyoto-u.ac.jp).

Fig. 1. An aerial photo of the MU radar operated by RISH, Kyoto University, in Shigaraki, Japan. The active phased array antenna has 475 Yagi elements and is 103 m in diameter.

of the zonal winds, a theory based on the effect of mechanical friction from wave breaking processes of atmospheric gravity waves was proposed.[7),8)]

In the 1980s a notable advance was made in understanding the role of atmospheric gravity waves in the dynamics of the middle atmosphere with the development of large atmospheric radars that detect the electromagnetic wave scattering caused by atmospheric turbulence.[9)] Research Institute for Sustainable Humanosphere (RISH) at Kyoto University, Japan, constructed the Middle and Upper atmosphere (MU) Radar at Shigaraki (34.85°N, 136.10°E), Japan in 1984.[10)] The MU radar transmits signals at a frequency of 46.5 MHz and at a peak transmission power of 1 MW.[11),12)] It is a versatile multi-purpose atmospheric radar with an active phased array antenna that is 103 m in diameter and contains 475 Yagi antenna elements (Fig. 1). The MU radar measures the wind velocity from near the Earth's surface up to an altitude of about 25 km, and at high altitudes between 60 and 90 km, with an altitude accuracy of several hundred meters and a time resolution of several minutes. It is also capable of measuring the characteristics of the ionosphere.[13)] The MU radar has enabled detailed observations of the behavior of the gravity waves,[14),15)] thus

greatly advancing our understanding of the middle atmosphere.

Generally, satellite radiometer measurements using thermal emission from the atmosphere were intended to analyze large-scale atmospheric phenomena so that the altitude resolution was not sufficient to capture the vertical profiles of atmospheric gravity waves.[16)] However, the zonal mean temperature variances attributed to atmospheric gravity waves in the stratosphere were observed with limb scanning infrared radiometer.[17)] A quantitative picture of the global distribution of atmospheric gravity waves has also been obtained through satellite-borne microwave radiometer observations as well.[18),19)] Recent advances in satellite-borne radiometers made it possible to analyze the behavior of meso-scale gravity waves.[20)] In addition, novel GPS radio occultation (GPS RO) techniques[21)] have been able to achieve measurement resolution and accuracy comparable to those of ground-based techniques such as the MU radar and balloon observations (radiosonde). GPS RO has provided a unique opportunity for us to understand the global distribution of atmospheric gravity wave activity.[22)]

This paper reviews the characteristics of atmospheric gravity waves in terms of their generation,

propagation, and dissipation processes by chiefly referring to the results from the MU radar and GPS RO measurements.

2. A linear theory of atmospheric gravity waves

We first consider the behavior of a monochromatic gravity wave in a frictionless, adiabatic, stably-stratified atmosphere in the context of the linear wave theory. Using the basic formulas for atmospheric dynamics; the equations of momentum, the law of mass conservation (continuity equation), and the second law of thermodynamics (equation of state), we can solve for small perturbations, whose variations are expressed by a harmonic function in time and space (horizontal and vertical).[1),2),23)] This results in a dispersion relationship between the horizontal wave number, k, in the wave propagation direction, the vertical wave number, m, and the frequency, ω.

$$m^2 = k^2(N^2 - \omega^2)/(\omega^2 - f^2) \qquad [1]$$

$$\omega = k(c - \bar{u}) \qquad [2]$$

Here, N is the frequency of oscillation determined by buoyancy effects due to stable stratification. It is called the Brunt–Väisälä or buoyancy frequency, and the corresponding oscillation period is approximately 10 minutes in the troposphere and about 5 minutes in the middle atmosphere. f is the inertial frequency due to the Coriolis force. It varies with latitude, with the corresponding inertial period given by 12 h/sin[latitude] in hours. For example, at 35° latitude, the inertial period is about 21 hours. $\bar{u}$ is the horizontal background wind velocity in the direction of the gravity wave propagation. For wave components that propagate vertically, the condition $m^2 > 0$ must be satisfied, so that their frequency must fall in the range: $N > \omega > f$.

3. Excitation of atmospheric gravity waves: A case study using the MU radar

Atmospheric gravity waves are generated by a variety of mechanisms that cause vertical displacements of air parcels, such as meteorological disturbances or cumulous convection within the troposphere, instability in jet streams, and the interactions of surface winds with topography.[3)]

When a stably stratified air flow encounters a mountain range as shown in Fig. 2, the air is lifted over the mountain, and oscillations are induced in the stream lines on the leeward side of the mountain.[23)] These meso-scale perturbations are known as mountain waves or orographic waves. The horizontal
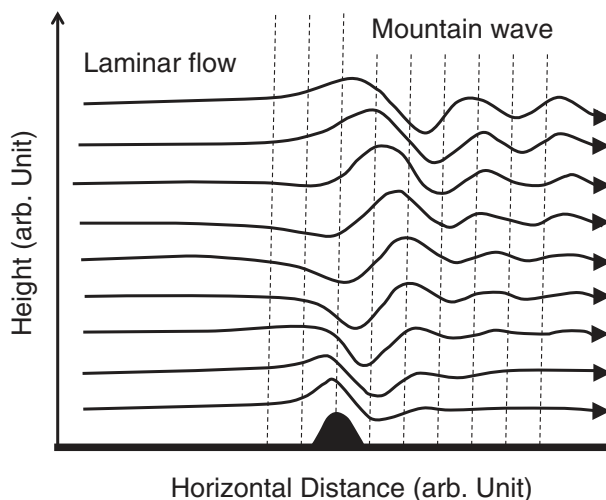

Fig. 2. Generation of mountain (orographic) waves by the interaction of stably stratified air flow with topography.[23)] Air parcels lifted up by the mountain give rise to gravity waves, which propagate and transfer their momentum and energy up into the middle atmosphere.

structure of mountain waves can be recognized in visible satellite imagery. For example, an animation of a mountain wave activity over the southern Rockies in New Mexico can be seen on the NOAA web page: http://www.srh.noaa.gov/abq/?n= features_mountainwaves.

Next, we show an example of gravity waves resulting from a meteorological disturbance, as observed by the MU radar. The MU radar can continuously measure all three components of wind velocity with height and time resolution of a few hundred meters and a few minutes, respectively. In addition, temperature profiles can be obtained with the radio acoustic sounding system (RASS),[24)] which measures the sound speed from the radar echo scattered by refractive index fluctuations generated by acoustic waves.

Figure 3 is a schematic diagram of the height-horizontal section of a cold front, where warm and cold air masses collide. The warm air mass is lifted above the cold air resulting in the development of a cumulous cloud over the cold front. We observed the passage of a cold front on August 3–4, 1991 using the MU radar with RASS.[25)] Figure 4 shows a contour plot of the temperature deviations from the mean values during the observation period, and the wind velocity vectors, combining the northward and vertical velocity components. Note that the horizontal axis, showing local time, is reversed. Assuming that the cold front moved eastward at a constant

speed, the observed height-time structure in Fig. 4 can be compared with the vertical section of the cold front in Fig. 3.

The structure of the cold front in Fig. 4 is consistent with the well-established model of a cold front shown in Fig. 3. As the cold air mass crept
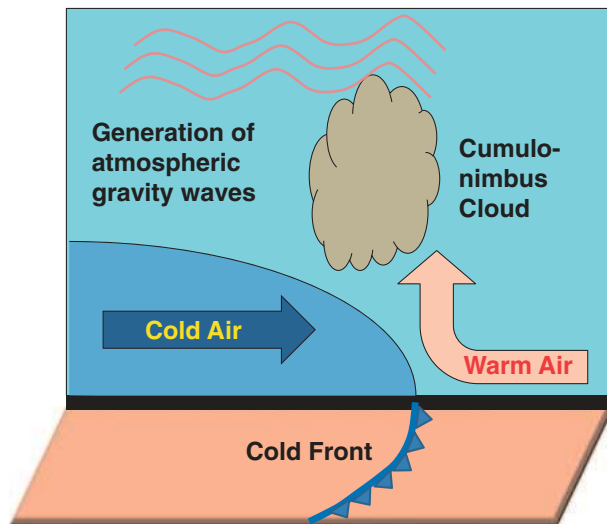

Fig. 3. A schematic cross section of a cold front. A height-horizontal cross section of the cold front depicts interaction between warm and cold air masses, which results in the generation of a cumulous cloud with precipitation. Atmospheric gravity waves are emitted because of such meteorological disturbances.

underneath the warm air, the warm air was uplifted at the forward side of the front. A remarkably strong upward wind was found between 21:00 and 22:00 LT below 2.5 km altitude. Then the warmer air was rapidly raised upward at around 20:00–21:00 LT. The vertical wind changed direction from upward to downward after around 22:30 LT, coinciding with a drastic change in the temperature structure.

A variety of temperature perturbations can also be seen in Fig. 4. A temperature decrease occurred rapidly within a few hours centered around 22:00–23:00 LT. There were also small-scale (10–20 min) periodic fluctuations embedded inside both the warm and cold air masses. These fluctuations were not random; rather, they show clear phase propagation with altitude. Oscillations in the vertical winds coincided with the temperature perturbations. The interaction between the cold and warm air masses was associated with rapid changes in wind velocity and temperature, resulting in emission of atmospheric gravity waves.

4. Role of gravity waves in the middle atmosphere dynamics

Much theoretical research has been conducted on the dynamical characteristics of atmospheric gravity waves, focusing mainly on the process by which gravity waves deposit their momentum and energy onto the background winds in the middle atmosphere.[3] We explain below two important
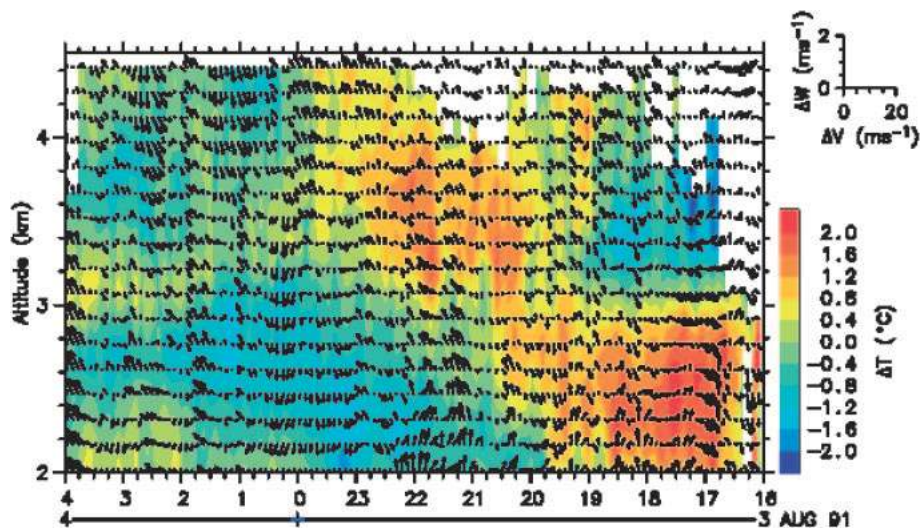

Fig. 4. A time-height section of a cold front observed by the MU radar with RASS on August 3–4, 1991.[25] Wind velocity and temperature were measured every three min with a height resolution of 150 m. Background contour shows the deviation of temperature from the mean values during the observation period. Vectors indicate a combination of vertical and northward wind velocity components.

processes to understand interaction between gravity waves and background mean zonal winds, the critical level interaction and convective instability.[26]

First, consider a scenario in which the background horizontal wind speed increases with altitude. An atmospheric gravity wave excited at a low altitude propagates upward and reaches an altitude at which its horizontal phase speed becomes equal to the horizontal background wind speed in the direction of propagation. The wave cannot pass above this altitude and becomes trapped there. This process does not necessarily directly cause the wave to attenuate, but while the wave remains at that altitude, it appears to attenuate due to nonlinear effects. This is referred to as critical level absorption.[27]

The atmospheric gravity waves attenuate due to unstable phenomena associated with shear or convection instabilities.[7),23),26)] Generally, shear instability, which is also known as Kelvin-Helmholtz Instability (KHI), occurs when the Richardson number, Ri, of the background horizontal wind velocity becomes smaller than 0.25. Note that Ri is an index of atmospheric stability, which is defined as a ratio of the vertical potential temperature gradient to the square of the wind shear.

Convective instability, on the other hand, occurs when Ri becomes negative, that is, when the temperature gradient becomes smaller than the adiabatic lapse rate and stratification becomes unstable. It is theoretically predicted that the instability of a gravity wave can be attributed mainly to convective instability for the high frequency components of gravity waves, and to shear instability for the low frequency components.[26] In the case of convective instability for a gravity wave, Ri has been shown to reach a minimum at the altitude where the horizontal wind velocity perturbations of gravity wave reaches its maximum. It is also estimated theoretically that short-period gravity waves carry momentum more efficiently, and that they are more effective in terms of mean flow acceleration/deceleration.[26]

Other dissipation processes of atmospheric gravity waves, though not described in detail here, include a change in their amplitude over time (referred to as "transience"), wave cascades due to the elastic interaction between waves, molecular viscosity and Newtonian radiative cooling.

4.1. Height profiles of atmospheric gravity waves from a coordinated observation. We now discuss changes in atmospheric gravity waves that occur when they propagate upward from the tropo-
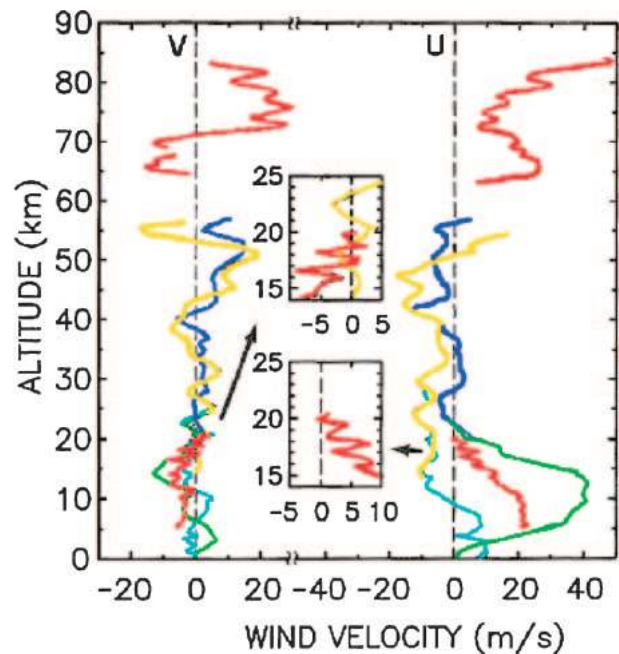

Fig. 5. Vertical profiles of the eastward (U, right panel) and northward (V, left panel) wind velocity measured simultaneously with the MU radar (red line), a rocketsonde at Uchinoura (yellow) and Ryori (blue), and routine balloon soundings (radiosonde) at Kagoshima (light blue) and Sendai (green). Note that the MU radar observed two altitude regions: 5–20 km and 65–85 km. The inset is an enlargement of the MU radar observations of the wind velocity.[29]

sphere to the overlying stratosphere and mesosphere. We show in Fig. 5 wind velocity profiles that were measured simultaneously with the MU radar [red lines in Fig. 5], radiosondes, and rocketsondes.[28),29)] Although these data were acquired simultaneously on September 11, 1985, observation sites were widely distributed over Japan. Yet, Fig. 5 is useful to obtain a perspective on the important characteristics of gravity waves in the entire middle atmosphere.

Figure 5 shows results from routine balloon soundings (radiosonde) launched from the weather stations of Japan Meteorological Agency (JMA) at Sendai (38.27°N, 140.90°E) [green] and Kagoshima (31.55°N, 130.55°E) [light blue], as well as meteorological rocket observation data from the Ryori Observatory (39.03°N, 141.83°E) [blue] of JMA. Profiles from an experimental rocket (MT135-44) [yellow line in Fig. 5] launched from the Japan Aerospace Exploration Agency (JAXA) Uchinoura Space Center (31.25°N, 131.08°E) are also shown. The zonal wind data at Sendai [green] on the right side of Fig. 5 shows a strong tropospheric jet stream at an altitude of approximately 10 km. The tropo-

spheric jet became weaker at the lower latitude stations, Shigaraki [red] and Kagoshima [light blue], because of the latitudinal variations in the vertical structure of the tropospheric jet.

Oscillations in wind velocity due to atmospheric gravity waves appear at all altitudes, as shown in Fig. 5. The MU radar measurement confirmed that a gravity wave is superimposed on the jet stream at an altitude of 15–25 km and had a vertical wavelength of about 2 km and an amplitude of 2–3 m/s (see the inset in Fig. 5). The standard data sets from routine radiosonde observations at Sendai and Kagoshima show wind velocity profiles at height intervals of several hundred meters (green and light blue), and therefore, were incapable of describing these gravity wave components clearly.

The wind velocity profile in the high-altitude range of 20 to 57 km is shown by the MT135-44 rocket (yellow) and the meteorological rocket at Ryori (blue). Fluctuations of about 5 km in the vertical wavelength and about 3 m/s in the wind speed amplitude are seen at an altitude of 20–30 km, and fluctuations of about 10 km in the vertical wavelength and 15 m/s in the wind velocity, at an altitude of 30–50 km. The MU radar observed the wind velocity in the mesosphere at an altitude of 65–85 km, which shows an atmospheric gravity wave with an estimated vertical wavelength of about 15 km. The magnitude of fluctuation in the wind velocity was nearly 25 m/s for the meridional and 10 m/s for the zonal components. Gravity waves with shorter wavelengths can also be seen superimposed on the dominant gravity wave in the mesosphere.

To summarize, Fig. 5 shows that the vertical wavelength of the gravity wave grew from 2–3 km in the lower stratosphere (altitude 15–25 km), to about 5 km in the upper stratosphere (altitude 30–50 km), and further increased to approximately 10–15 km in the mesosphere (altitude 60–90 km).[29] These oscillations did not originate from a single wave, that is, observations were not a continuous tracking of the same wave. However, we can see that different waves with different vertical wavelengths were clearly dominant at different altitudes.

Gravity waves appear as a disturbances or noise in the wind velocity field in the lower atmosphere (troposphere). However, as they propagate upward through the middle atmosphere, their amplitude increases such that the associated horizontal wind velocity becomes large enough to exceed the mean background wind in the mesosphere. The energy of atmospheric gravity waves is proportional to the product of the atmospheric density and the square of the amplitude of the wind velocity fluctuation. Since the atmospheric density diminishes exponentially with altitude with e-folding length scale of about 8 km, the amplitude of an atmospheric gravity wave should also increase exponentially if the wave were propagating upwards without any dissipation. For example, an altitude change of 60 km would yield an increase in amplitude by a factor of 43. However, the observed rate of increase in Fig. 5 was markedly smaller than this. This implies that the growth in amplitude of individual atmospheric gravity waves is restricted, suggesting wave attenuation during their upward propagation.

4.2. Breaking of gravity waves in the mesosphere. We used the MU radar to observe the atmospheric turbulence layers and the fluctuations in wind velocity simultaneously in order to investigate how the instability caused by gravity waves leads to turbulence. In the wind velocity profile in Fig. 6 (red lines), fluctuations due to a gravity wave with a vertical wavelength of about 10 km can be seen at an altitude of 70–80 km. With time, the region of strong vertical wind shear associated with the gravity wave tends to descend. According to the linear theory, the vertical group velocity at which energy propagates is opposite to the vertical phase velocity.[1),2)] As the gravity wave depicted in Fig. 6 shows downward phase progression, this wave appears to be generated in the lower atmosphere, and its energy is propagating upward.

Meanwhile, the turbulence echo shown in Fig. 6 (contour plots) exhibit a layered structure with a thickness of about 2–5 km at an altitude of 70–80 km. The altitude of this turbulence layer appears to decrease in synchrony with the wind shear. Note that the echo at 65 km stayed at a constant altitude because it is caused by a partial reflection.

To summarize, the atmospheric gravity wave showed a downward phase propagation over time, and the turbulence layer appeared to move down as well. Using the linear dispersion relationship for atmospheric gravity waves, the fluctuations in temperature can be inferred from the observed wind velocity, from which we can further estimate the Ri number including the effects of gravity waves. The MU radar observations indicated that a layer of strong turbulence is present at altitudes where Ri is small enough to induce the convective and/or shear instabilities.[30]

These above results suggest that the turbulent layer in the mesosphere is caused by the breaking of
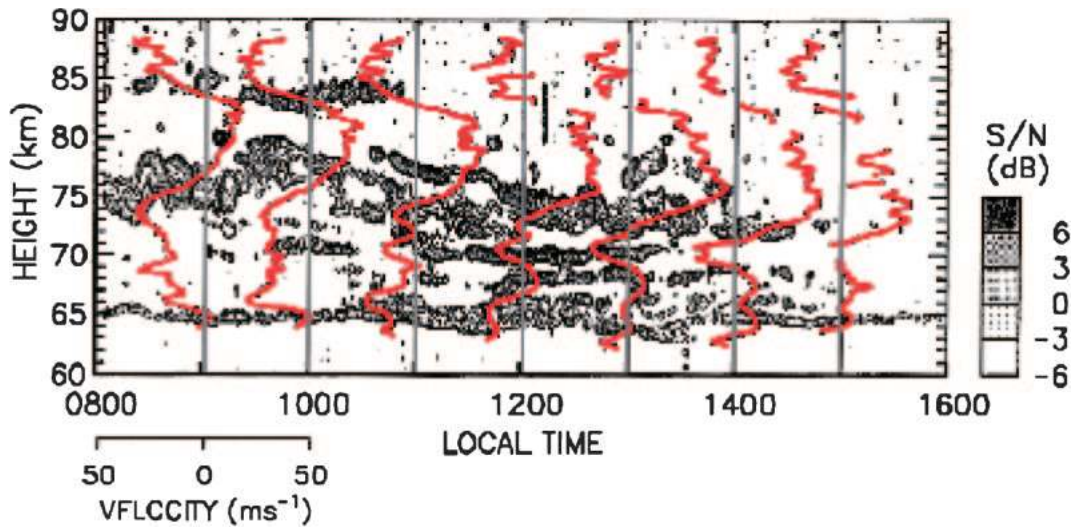
Fig. 6.   MU radar observations of time-height sections of atmospheric turbulence echo intensity (contour plot) and hourly profiles of the eastward wind velocity (red solid line) in the mesosphere (60–90 km altitude) during the daytime (8 am–4 pm) on October 18, 1986.
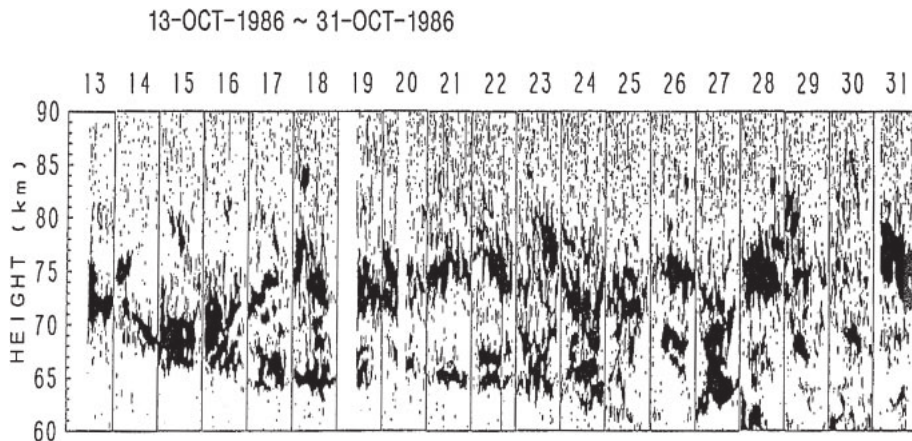

Fig. 7.   Time-height sections of the turbulence scattering echo intensity observed at 60–90 km in the mesosphere by the MU radar during daytime (8 am–4 pm) from October 13 to 31, 1986. Each small panel corresponds to the daily determinations, as in Fig. 6.

atmospheric gravity waves. Figure 7 shows the time and altitude distribution of turbulence echoes observed with the MU radar from October 13 to October 31, 1986. Note that the numerous points appearing above altitude 80 km are echoes from meteor trails. Figure 6 corresponds to the small panel in the sixth frame from the left in Fig. 7. Since the electron density in the mesosphere is extremely low at night, the turbulence scattering by electrons can only be detected during the day. Figure 7 therefore shows the turbulence echoes observed each day only between 8:00 am and 4:00 pm, so each panel in Fig. 7 is not contiguous with its adjacent panels. There is a 16 hour interval between adjacent panels.

Nevertheless, the figure clearly shows the turbulence layer appearing at a similar altitude for a period of over 10 days. Figure 7 also suggests interaction between larger scale atmospheric waves, such as atmospheric tides and planetary waves, and gravity waves, with resultant breaking of the gravity wave and formation of the turbulence layer. Superimposition of large-scale waves and the gravity waves appears to produce a persistent layer of low stability, where the instability phenomena and turbulence layers are concentrated.

4.3. Role of gravity waves in maintaining the middle atmosphere general circulation.   We describe next the dynamical friction effects caused by
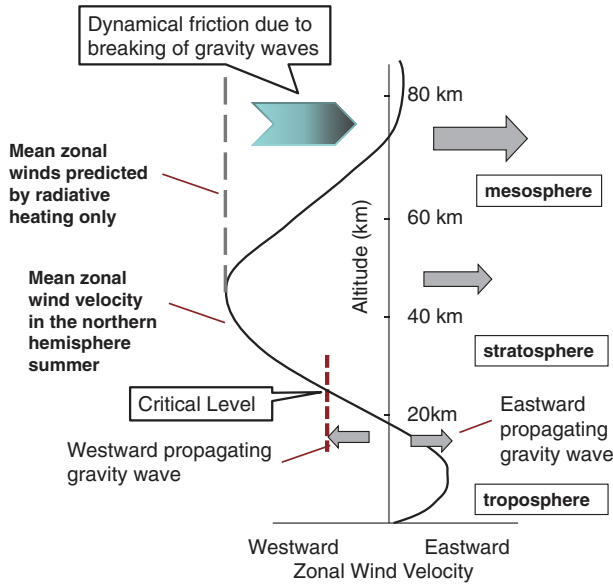
Fig. 8.   A schematic diagram depicting the fundamental concepts of interaction between mean winds and gravity waves. The solid line corresponds to a realistic profile of the zonal winds, while the dashed line indicates a profile considering the radiative balance alone. Thick arrows represent gravity waves.

gravity wave breaking, which decelerate the background mean zonal winds in the middle atmosphere. The latitudinal temperature gradient in the middle atmosphere due to solar heating gives rise to a zonal jet stream, which blows towards the west in summer (and the east in winter) in the northern hemisphere above an altitude of about 20 km, as shown in Fig. 8. Gravity waves excited in the troposphere have no preferred direction and so propagate in all horizontal directions. The wave components propagating toward the west will reach the critical level below about 40 km altitude because of the presence of the jet stream, and these waves will eventually be attenuated. The wave components propagating toward have no critical level to encounter and can continue to propagate upward into the mesosphere, and with increasing the wave amplitude. In the mesosphere, these atmospheric waves become large enough to distort the background wind velocity and the thermal structure significantly. Combination of the vertical wind shear due to gravity waves and the background shear causes a region of very low atmospheric stability. Convective instability ensues, producing turbulence as shown in Fig. 6. The gravity waves break and deposit their horizontal momentum onto the background mean winds.[26] In winter, the jet stream direction in the middle atmosphere is reverse

of that depicted in Fig. 8 and the deceleration occurs toward the west in the mesosphere.

MU radar observations showed the upward flux of momentum, $\rho_0 u'w'$ at 60–85 km, where ρ_0 is the mean atmospheric density.[31] The zonal momentum flux showed eastward maxima in summer and westward maxima in winter months. From the height derivative of the momentum flux, the acceleration at 70 km altitude was calculated to be eastward at 7 to 13 m/s per day in summer and westward at 8 to 11 m/s per day in winter, in good agreement with theoretical predictions.

5. Frequency and vertical wave number spectra of atmospheric gravity waves

Atmospheric gravity waves are seldom monochromatic in the real atmosphere. The observed fluctuations due to gravity waves are complex, with many imbedded wave components. It is therefore useful to analyze the frequency and the vertical wave number spectra of wind velocity and temperature fluctuations.[32] Vertical wave number spectra can be analyzed using high resolution profiles from meteorological balloon (radiosonde) observations and high precision satellite data, such as GPS radio occultation. Atmospheric radars can perform continuous observation of wind velocity fluctuations with excellent time and vertical resolution, and are therefore, also well-suited for analysis of the frequency and vertical wave number spectra.[33],[34]

5.1. Frequency spectra.   First, we introduce a semi-empirical model for the frequency spectrum of atmospheric gravity waves.[32],[35] When the wave frequency ω satisfies the condition, $N \gg \omega \gg f$, as it should for vertically propagating atmospheric gravity waves, the spectral density of the horizontal wave velocity perturbation u' can be approximated by $\omega^{-5/3}$. Considering the dispersion relationship in Eq. [1], the corresponding frequency spectrum for the vertical wind velocity w' can be expressed as $\omega^{1/3}$. This spectral model has been determined more or less empirically,[35] but it nevertheless agrees very well with the observations regardless of location, altitude range, and season. It should be noted, however, that although this spectrum bears some resemblance to the formulas for the three-dimensional isotropic turbulence spectra in the inertial subrange, it is unrelated to turbulence.

5.2. Vertical wave number spectrum for a quasi-monochromatic wave.   A theory that fully explains the spectra of atmospheric gravity waves has not yet been developed, but, there has been some

explanation of the form of the high wave number portion of the vertical wave number spectra. We will now focus on the dissipation of atmospheric gravity waves due to convective instability, from which we can deduce the corresponding saturated vertical wave number spectra.[36)]

When a gravity wave breaks because of convective instability, its amplitude is suppressed to a certain level. Therefore, this phenomenon is called wave saturation.[36)] In the dispersion relationship of Eq. [1], where $N \gg \omega \gg f$, we obtain:

$$|m| = N/|c - \bar{u}| \qquad [3]$$

Since the potential temperature θ contains a fluctuation portion θ' attributed to the gravity wave, we assume that convective instability will occur when the vertical gradient $\mathrm{d}(\bar{\theta} + \theta')/\mathrm{d}z$ becomes negative, where $\bar{\theta}$ is the background potential temperature. This is equivalent to the following condition for the magnitude of the wind velocity perturbation due to the gravity wave u':

$$u' > |c - \bar{u}| \qquad [4]$$

Therefore, at the limit of convective instability, the amplitude of the gravity wave is suppressed to the following value:

$$u' = N/|m| \qquad [5]$$

As a result, the amplitude of the gravity wave ceases to grow with altitude, appearing to have reached a state of saturation. The energy per unit mass of a monochromatic gravity wave is defined by $N^2/2m^2$. The wave energy can be obtained by multiplying this value by the atmospheric density. When the gravity wave reaches the saturation altitude, the wave perturbation amplitudes stay constant with altitude. So, in accordance with the decrease in atmospheric density the wave energy decreases exponentially with altitude.

For an ideal monochromatic sinusoidal wave, the wave number spectrum width Δm is zero, and, the corresponding spectrum density, that is, the energy of a gravity wave per unit wave number at the central wave number, will be infinite. However, the spatial scale of a wave, $i.e.$, the number of wave cycles in the atmosphere, is always limited. Therefore, we can obtain finite values for both the spectral density and the band width Δm occupied by the wave. For a quasi-monochromatic gravity wave, Δm is empirically taken to be proportional to its central wave number m, although theoretical explanation for this is not robust.[36),37)] Under the assumption

$\Delta m \propto m$, the vertical wave number spectral density becomes proportional to $N^2/2m^3$.[36)]

Once we accept the proportionality between Δm and m, it provides an interesting insight into the form of the wave amplitude envelope for a saturated gravity wave. Consider amplitude modulation of a sinusoidal signal, whose characteristics are determined by the spectral distribution around the central wave number m. Because the ratio $\Delta m/m$ is constant for all wave components, the asymptotic envelope of a gravity wave becomes similar for all wave components. That is, if the vertical profile of a gravity wave is normalized by its vertical wavelength, it becomes similar regardless of the wavelength. In other words, number of wave cycles becomes the same for all saturated gravity waves.

5.3. Vertical wave number spectra for overlapping waves. We have so far discussed only the spectrum for a quasi-monochromatic wave. We now consider superposition of many waves with different vertical wave numbers in order to obtain a continuous wave number spectrum.

Let us consider the wind velocity perturbations, u_1 and u_2 attributed to two gravity waves of different vertical wavelengths, as shown in Fig. 9. The amplitude of perturbations due to gravity waves grows exponentially with height as the wave propagates upward. The magnitude of the wind shear, $|\mathrm{d}u/\mathrm{d}z|$, also increases with altitude, but at a faster rate for the shorter wavelength. When this exceeds a threshold value, the wave becomes unstable and ceases to grow.[38)] Figure 9 indicates that waves of shorter wavelength, u_2, become unstable at lower altitudes, and their amplitude is suppressed (saturated) as in Eq. [5].

In the previous section, we showed that the spectral density is proportional to m^{-3} for saturated gravity waves with large wave numbers, $i.e.$, for waves with short wavelengths. We assume that the spectral density is independent of wave number at small wave numbers, $i.e.$, for long wavelengths, and this portion of the spectrum must be smoothly connected with m^{-3} at large wave numbers.

We assumed that convective instability occurs when the vertical gradient of potential temperature, including the effect of the gravity wave, $\mathrm{d}\theta/\mathrm{d}z$, becomes negative. This should also hold true when multiple gravity waves overlap linearly. It is known that for a monochromatic sinusoidal wave, the variance (r.m.s. value) of the perturbations is equal to half the mean square of the peak value of the perturbations. We assume this relation can be
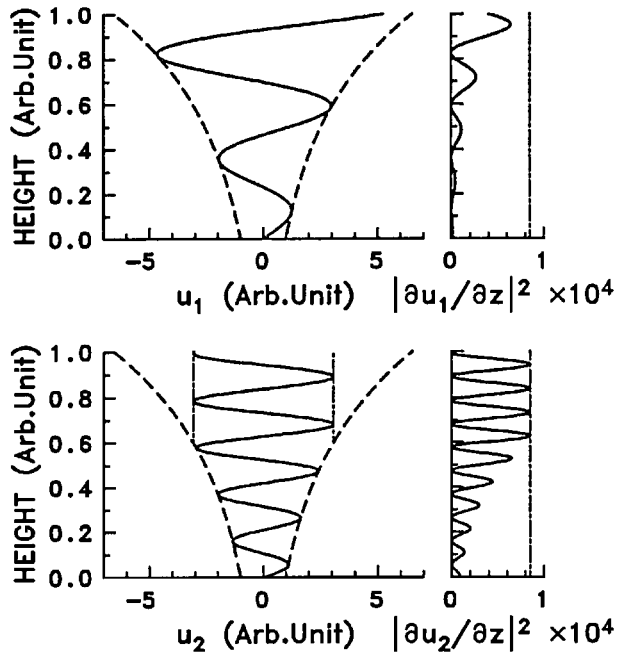
Fig. 9. A conceptual profile for the amplitude growth of horizontal wind velocity for upward propagating gravity waves with long (top) and short (bottom) vertical wavelengths.[38] The vertical gradients of the wind velocity are also compared in the right panels.
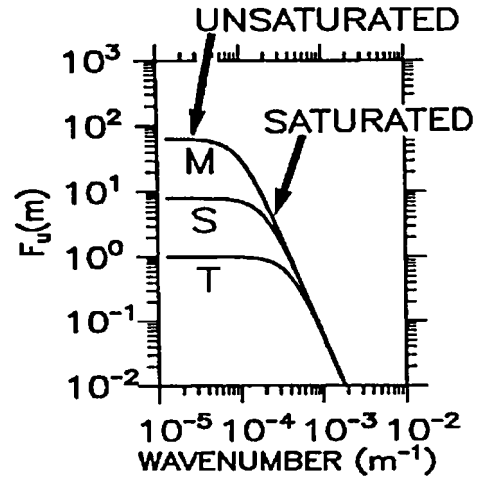

Fig. 10. A model of a vertical wave number spectrum for saturated gravity waves in the troposphere (T), stratosphere (S) and mesosphere (M). The spectral density in low wave numbers (unsaturated) increase with altitude ranges, while that in high wave number portion does not change, as the waves are saturated.

applied for the case with superposition of many gravity waves.[36] We can determine a coefficient of the spectrum that will make this variance equal to the integral value of the entire vertical wave number spectrum. The vertical wave number spectrum of θ'/θ_0 can be defined by the function $F_\theta(m)$ as follows:[33),39]

$$\mathrm{F}_\theta(\mathrm{m}) = \frac{1}{10g^2} \frac{N^4}{m^3} \qquad [6]$$

Further, the linear dispersion relation for a gravity wave can be used to determine the vertical wave number spectrum for the horizontal wind velocity fluctuation u':[36]

$$\mathrm{F}_u(\mathrm{m}) = \frac{1}{6} \frac{N^2}{m^3} \qquad [7]$$

These equations show that if an atmospheric gravity wave is saturated by convective instability, then, for sufficiently large values of m, the vertical wave number spectrum of the fluctuations in horizontal wind velocity and temperature caused by a gravity wave can be approximated by m^{-3}. The spectral density will be determined by the N^2 of the background atmosphere. Even where the convective instability phenomena cannot be clearly observed for individual waves, statistical analysis using the vertical wave number spectra enables us to understand the wave attenuation process.

Figure 10 shows the model vertical wave number spectra. The model spectra correspond to spectra from low to high altitudes through the troposphere (T), stratosphere (S), and mesosphere (M). The high wave number area on the right hand side takes the form of the saturated spectra, m^{-3}. Meanwhile, the low wave number region on the left hand side is unsaturated and the energy density per unit mass increases with altitude.

Figure 11 shows an example of vertical wave number spectra for the zonal and meridional wind velocity components observed by the MU radar.[34] As predicted, the high wave number shape is a good match with m^{-3}. The model exhibits different N^2 values for the troposphere and middle atmosphere, and, it is in good quantitative agreement with observed spectra in the middle atmosphere (stratosphere and mesosphere). In the troposphere, however, the observed spectra exceed the model values. This is likely due to the presence of other wind velocity disturbances, such as convection, and meteorological events in the lower atmosphere in addition to gravity waves.[34]

Observed wind velocity profiles (Fig. 5) show that the dominant vertical wavelength of the atmospheric gravity wave increases with altitude.[29]
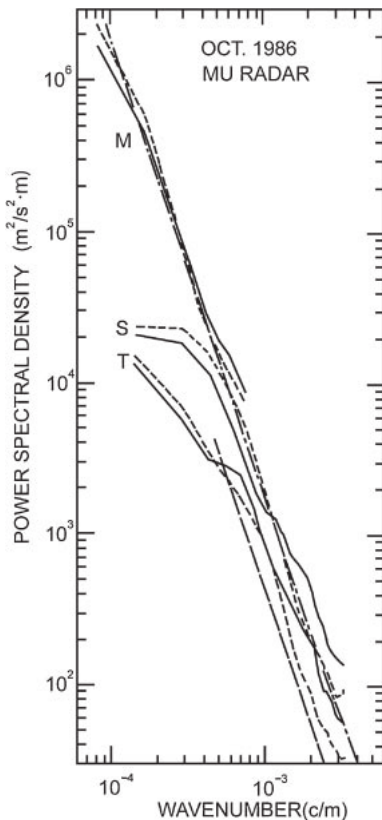
Fig. 11. Vertical wave number spectra of horizontal wind velocity in the mesosphere (M), stratosphere (S), and troposphere (T) observed with the MU radar in October 1986. The solid lines correspond to the zonal component of wind velocity, while the broken lines correspond to the meridional component of wind velocity. The straight dashed lines indicate the saturated spectral model in M, S, and T.[34]

This can be explained using the saturated spectrum. Generally, in a spectrum where wave number and spectral density are plotted on a log-log scale, the wave energy is the greatest at the wave number where the spectrum slope is -1, that is, m^{-1}. In Fig. 10, the wave component with the greatest energy is at the wave number where the spectral shape changes from m^0 to m^{-3}.

Figure 9 indicates that the gravity waves with large vertical wave numbers (short wavelengths) experience convective instability even at small amplitudes, and are saturated easily at low altitudes. Therefore, as shown in Figs. 10 and 11, the spectra are suppressed gradually from the high wave number side until the saturation value is reached. In the saturated portion, the amplitude stays constant regardless of the altitude. In the low wave number portion, the wave is not saturated, and the energy

density increases with altitude. Figure 10 suggests that the wave component about to reach saturation has the greatest energy and is dominant within the altitude profile. It also shows that the peak wave number shifts to the low wave number side as altitude increases. Therefore, at a higher altitude, the vertical wavelength of the prevailing atmospheric gravity wave increases considerably as seen in Fig. 5. Specifically, comparing the dominant gravity wave in Fig. 5 at the tropopause (about 10 km) and the mesosphere (60–90 km), we find the wave amplitude and the vertical wavelength have increased by a factor of about 10 and 5, respectively, which is consistent with the saturated spectral model.

6. Global distribution of the gravity wave activity using GPS radio occultation data

In this section, we show the global distribution of the gravity wave activity using satellite data, and discuss various wave excitation mechanisms. We employ here GPS radio occultation (RO) data that can achieve an altitude resolution similar to that of ground-based observations. GPS RO can provide temperature profiles from the ground up to altitudes of about 40 km. This data-set has been used to analyze the global distribution of atmospheric gravity wave energy.[22]

6.1. Principles of the GPS radio occultation method. We briefly explain basic concept of GPS-RO.[21),40)] Consider a GPS receiver on board a low Earth orbiting (LEO) satellite that is located on opposite side of the Earth's limb relative to a GPS satellite. When the radio signal from the GPS satellite to the LEO satellite traverses the Earth's atmosphere, it is refracted by the vertical gradient of atmospheric refractivity. From the LEO satellite, the GPS satellite appears to be below the horizon, and this is called occultation. Because of bending and propagation delay of the GPS radio waves within the atmosphere, a positioning error is generated. This error, however, can be used to infer atmospheric parameters.

Time interval between transmission and reception gives the actual propagation path length, while the straight distance can be estimated from coordinates of both satellites. By assuming spherical homogeneity of the Earth' atmosphere, the bending angle of the ray path can be calculated from geometrical configuration. Orbital motion of both transmitter and receiver produces the limb scanning geometry. As the bending angle is directly related to the vertical gradient of refractive index, the changes

in bending angle with the height of the ray tangent can be converted to a refractive index profile. In an actual retrieval procedure, the time derivative of the observed propagation phase delay is calculated. This Doppler effect is connected with orbiting velocity of GPS and LEO satellites projected onto the ray path, so that it is related to the bending angle of the ray path.

Refractivity profile can then be used to derive profiles of atmospheric density from the troposphere to the mesosphere. In the dry atmosphere above about 10 km, the refractive index is related solely to the atmospheric temperature by assuming a hydrostatic equilibrium. Water vapor also makes a significant contribution to refractivity in the lower troposphere, so that temperature and humidity are retrieved by referring to a model standard atmosphere. In an ionized atmosphere, a profile of electron density can also be obtained from the refractive index profile.[40] The GPS-RO technique thus provides a unique opportunity to observe the global morphology of atmospheric gravity waves, by taking advantage of superior vertical resolutions of approximately 200 m. As a limb sounder, the along-track horizontal resolution is approximately 300 km.

In 1995, the first GPS RO mission called GPS/MET (GPS/Meteorology)[21] was conducted by the University Corporation for Atmospheric Research (UCAR) in collaboration with Jet Propulsion Laboratory (JPL). A number of GPS-RO missions such as CHAMP and SAC-C in 2001 were carried out since that very successful experiment. As a joint project between UCAR and the National Space Organization (NSPO), Taiwan, the COSMIC/FORMOSAT3 mission was launched in 2006 using six LEO satellites.[41] Installing radio occultation antennas on the fore and aft of a single LEO satellite provides temperature profiles 300–400 times per day, and COSMIC produces about 2,500 data points per day from the GPS constellation.

6.2. Global distribution of gravity waves from GPS radio occultation data. The temperature data obtained via GPS RO offers outstanding altitude resolution, which makes it possible to analyze medium-scale temperature disturbances in the stratosphere due to atmospheric gravity waves. Since the coverage includes areas over the ocean as well as the southern hemisphere, where ground-based observations have been sparse, GPS RO enables us to investigate the previously unexplored global characteristics of atmospheric gravity waves.

Figure 12(a) shows the results of a gravity wave energy analysis using GPS/MET data.[22] The wave component of vertical wavelengths shorter than 10 km was extracted for the altitude of 20–30 km. The gravity wave energy appears to be greater in the equatorial region. Notably, it expands above the region from Indonesia across to the Indian Ocean, Africa, and the Amazon. Figure 12(b) shows satellite measurements of the infrared radiation from cloud tops (out-going long-wave radiation, OLR) indicating strong cumulous activity over these regions. Therefore, in the equatorial region, cumulous convection appears to be an important excitation mechanism for atmospheric gravity waves.

Figure 13 shows a meridional section of the gravity wave energy analyzed using COSMIC GPS RO data from December 2006.[42] As noted above, the wave energy is particularly high in the equatorial region. At the mid-latitudes in winter, waves appear to grow actively along the winter jet stream, which is consistent with earlier MU radar observations.[43] In the northern polar region, wave energy is highly concentrated at altitudes above 25 km, which is related to the behavior of the polar vortex.[44]

Figure 14 shows a schematic diagram of the characteristics of equatorial atmosphere dynamics.[45] Cumulous convections are actively generated due to intense solar heating in the tropics. They in turn excite atmospheric gravity waves, which propagate upward carrying momentum and energy. As already discussed in Section 4.3, the interaction of the gravity waves with the background mean zonal winds plays an important role in the middle atmosphere dynamics. The gravity waves can even penetrate up to the ionosphere, where they trigger ionospheric irregularities.

7. Conclusions

We presented a brief review of the current understanding of atmospheric gravity waves. The wave breaking process, which plays an important role in determining the general circulation of the middle atmosphere, was examined in detail. We first discussed a simple linear theory for wave breaking due to convective instability. We also derived a vertical wave number spectrum model for saturated gravity waves. Using precise ground-based measurements with the MU radar, we studied the behavior of the atmospheric gravity waves. In particular, we investigated the saturation of gravity waves, which leads to wave attenuation and turbulence generation.
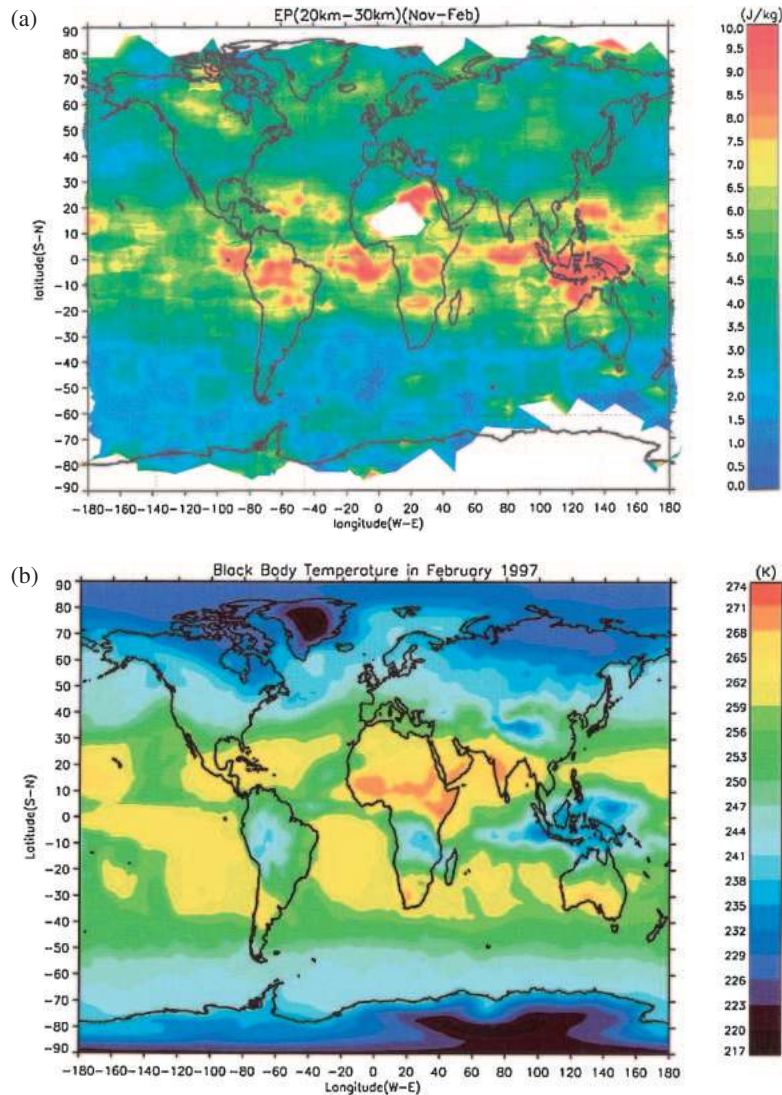
Fig. 12. (a) Global distribution of gravity wave energy analyzed during winter in the northern hemisphere (Nov.–Feb. in 1995–1997) using GPS radio occultation data from GPS/MET.[22] Warm colors (yellow-orange-red) correspond to intense wave activity. Data for the African region is lacking (white). (b) Distribution of cloud top temperature from satellite measurement of out-going long-wave radiation (OLR) with an infrared radiometer. The bluish region at low latitudes indicates the existence of tall clouds.

We showed that the MU radar observations are consistent with theoretical predictions.

Using GPS/MET and COSMIC GPS radio occultation data, we studied the climatological behavior of atmospheric gravity waves in the stratosphere. The gravity wave energy was shown to be enhanced over the tropics, indicating active wave generation due to cumulous convection. Tropospheric jet and polar night jet were also shown to be important excitation sources, in addition to the interaction of mean flow with topography.

Observational studies show that atmospheric gravity waves are excited by a variety of mechanisms and occur constantly all over the globe. When these waves propagate upward, they transport energy and momentum upward from the troposphere, thus playing an important role in driving the general atmospheric circulation in the middle atmosphere. The effects of atmospheric gravity waves are incorporated into the general circulation model (GCM) to greatly improve the forecasting accuracy.[46]
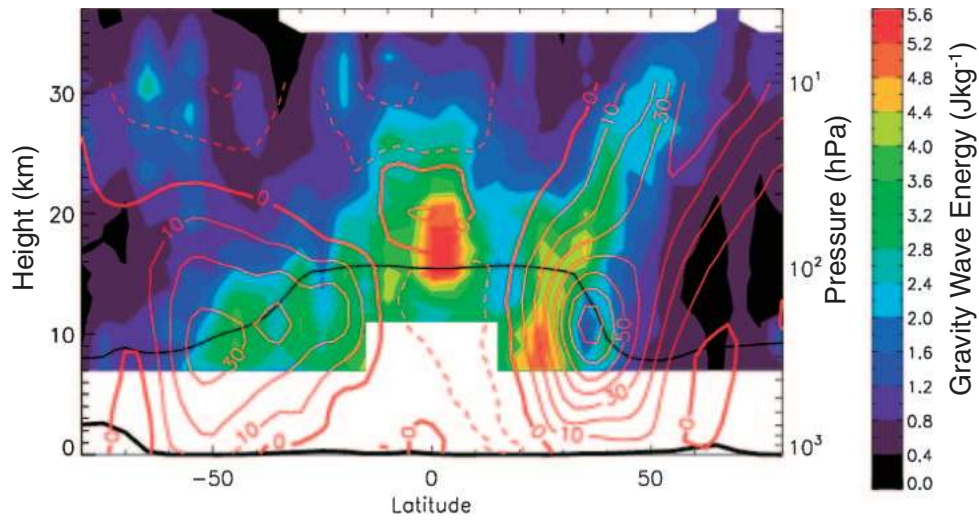
Fig. 13. A latitude-altitude section of the distribution of atmospheric gravity wave energy for vertical wavelengths shorter than 7 km taken from temperature data from COSMIC GPS radio occultation. The longitudinal position of the observations is centered on 140° E, including Japan. The red line indicates the background zonal wind with a strong winter jet stream. The line near altitude 10–15 km indicates the tropopause. The black line at the bottom indicates topography (elevation above sea level).[42]
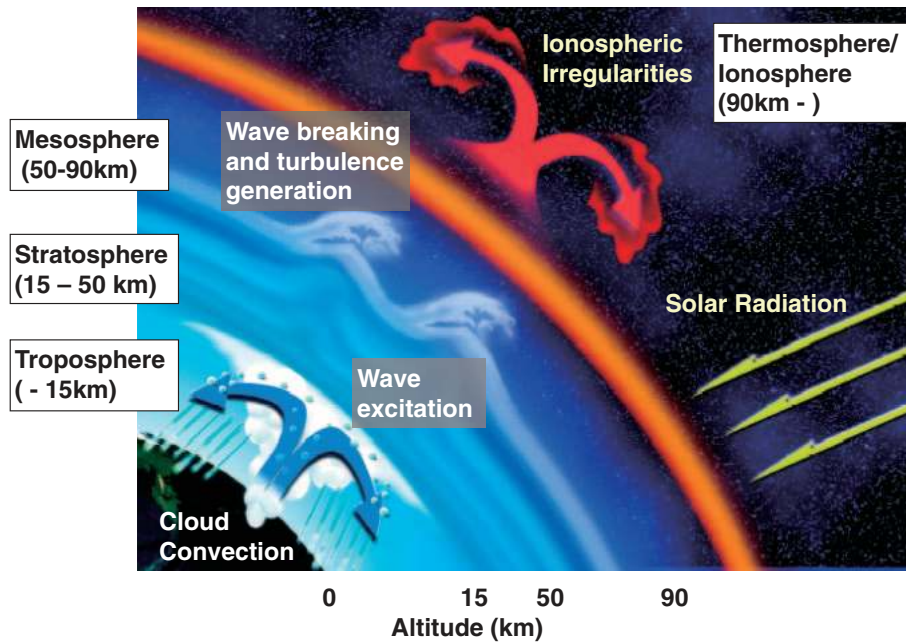

Fig. 14. Atmospheric coupling processes in the equatorial atmosphere.[45]

References

1) Hines, C.O. (1960) Internal atmospheric gravity waves at ionospheric heights. Can. J. Phys. **38** (11), 1441–1481.

2) Hines, C.O. (1963) The upper atmosphere in motion. Q. J. R. Meteorol. Soc. **89**, 1–42.

3) Fritts, D.C. and Alexander, M.J. (2003) Gravity wave dynamics and effects in the middle atmosphere. Rev. Geophys. **41**, doi:10.1029/2001RG000106.

4) Leovy, C. (1964) Simple models of thermally driven mesospheric circulation. J. Atmos. Sci. **21**, 327–341.

5) CIRA72 (1972) COSPAR International Reference Atmosphere, Akademie-Verlag, Berlin.

6) Holton, J.R. (1983) The influence of gravity wave breaking on the general circulation of the middle atmosphere. J. Atmos. Sci. **40**, 2497–2507.

7) Lindzen, R.S. (1981) Turbulence and stress due to gravity wave and tidal breakdown. J. Geophys. Res. **86**, 9707–9714.

8) Matsuno, T. (1982) A quasi-one-dimensional model of the middle atmospheric circulation interacting with internal gravity waves. J. Meteorol. Soc. Jpn. **60**, 215–226.

9) Balsley, B.B. and Gage, K.S. (1980) The MST radar technique: Potential for the middle atmospheric studies. Rev. Pure Appl. Geophys. **118**, 459–493.

10) Kato, S., Ogawa, T., Tsuda, T., Sato, T., Kimura, I. and Fukao, S. (1984) The middle and upper atmosphere radar: First results using a partial system. Radio Sci. **19**, 1475–1484.

11) Fukao, S., Sato, T., Tsuda, T., Kato, S., Wakasugi, K. and Makihira, T. (1985) The MU radar with an active phased array: 1. Antenna and power amplifiers. Radio Sci. **20**, 1155–1168.

12) Fukao, S., Tsuda, T., Sato, T., Kato, S., Wakasugi, K. and Makihira, T. (1985) The MU radar with an active phased array: 2. In-house equipment. Radio Sci. **20**, 1169–1176.

13) Fukao, S., Kelley, M.C., Shirakawa, T., Takami, T., Yamamoto, M., Tsuda, T. and Kato, S. (1991) Turbulent upwelling of the mid-latitude ionosphere, 1. Observational results by the MU radar. J. Geophys. Res. **96**, 3725–3746.

14) Tsuda, T., Kato, S., Yokoi, T., Inoue, T., Yamamoto, M., VanZandt, T.E., Fukao, S. and Sato, T. (1990) Gravity waves in the mesosphere observed with the middle and upper atmosphere radar. Radio Sci. **25**, 1005–1018.

15) Sato, K. (1993) Small scale wind disturbances observed by the MU radar during the passage of typhoon Kelly. J. Atmos. Sci. **50**, 518–537.

16) Alexander, M.J. (1993) Interpretations of observed climatological patterns in stratospheric gravity wave variance. J. Geophys. Res. **103**, 8627–8640.

17) Fetzer, E. and Gille, J.C. (1996) Gravity wave variance in LIMS temperatures. 2. Comparison with the zonal-mean momentum balance. J. Atmos. Sci. **53**, 398–410.

18) Wu, D.L. and Waters, J.W. (1996) Satellite observations of atmospheric variances: A possible indication of gravity waves. Geophys. Res. Lett. **23**, 3631–3634.

19) Preusse, P., Schaeler, B., Bacmeister, J.T. and Offermann, D. (1999) Evidence of gravity waves in CRISTA temperatures. Adv. Space Res. **24**, 1601–1604.

20) Ern, M., Preusse, P., Alexander, M.J. and Warner, C.D. (2004) Absolute values of gravity wave momentum flux derived from satellite data. J. Geophys. Res. **109**, doi:10.1029/2004JD004752.

21) Ware, R., Rocken, C., Solheim, F., Exner, M., Schreiner, W., Anthes, R., Feng, D., Herman, B., Gorbunov, M., Sokolovskiy, S., Hardy, K., Kuo, Y., Zou, X., Trenberth, K., Meehan, T., Melbourne, W. and Businger, S. (1996) GPS sounding of the atmosphere from low Earth orbit: Preliminary results. Bull. Am. Meteorol. Soc. **77**, 19–40.

22) Tsuda, T., Nishida, M., Rocken, C. and Ware, R.H. (2000) A global morphology of gravity wave activity in the stratosphere revealed by the GPS occultation data (GPS/MET). J. Geophys. Res. **105**, 7257–7273.

23) Gossard, E.E., and Hooke, W.H. (1975) Waves in the atmosphere: Atmospheric Infrasound and Gravity Waves: Their Generation and Propagation. Elsevier Sci. Pub. Co., Amsterdam and New York.

24) Matuura, N., Masuda, Y., Inuki, H., Kato, S., Fukao, S., Sato, T. and Tsuda, T. (1986) Radio acoustic measurement of temperature profile in the troposphere and lower stratosphere. Nature **323**, 426–428.

25) Adachi, T. (1996) Detailed temperature structure of meteorological disturbances observed with RASS, Ph.D thesis, Kyoto University.

26) Fritts, D.C. (1984) Gravity wave saturation in the middle atmosphere: A review of theory and observations. Rev. Geophys. Space Phys. **22**, 275–308.

27) Booker, J. and Bretherton, F.P. (1967) The critical layer for unternal gravity waves. J. Fluid Mech. **27**, 513–539.

28) Tsuda, T., Murayama, Y., Oyama, K.-I., Schmidlin, F.J., Bittner, M., Kanzawa, H., Nakamura, T., Yamanaka, M.D., Fukao, S. and Kato, S. (1992) Rocketsonde observations of the middle atmosphere dynamics at Uchinoura (31°N, 131°E) during DYANA campaign. Part II: Characteristics of gravity waves. J. Geomag. Geoelectr. **44**, 1009–1023.

29) Murayama, Y., Tsuda, T., Yamamoto, M., Nakamura, T., Sato, T., Kato, S. and Fukao, S. (1992) Dominant vertical scales of gravity waves in the middle atmosphere observed with the MU radar and rocketsondes. J. Atmos. Terr. Phys. **54**, 339–346.

30) Yamamoto, M., Tsuda, T., Kato, S., Sato, T. and Fukao, S. (1987) A saturated inertia gravity wave in the mesosphere observed by the Middle and Upper Atmosphere Radar. J. Geophys. Res. **92**, 11993–11999.

31) Tsuda, T., Murayama, Y., Yamamoto, M., Kato, S. and Fukao, S. (1990) Seasonal variation of momentum flux in the mesosphere observed with the MU radar. Geophys. Res. Lett. **17**, 725–728.

32) VanZandt, T.E. (1982) A universal spectrum of

buoyancy waves in the atmosphere. Geophys. Res. Lett. **9**, 575–578.

33) Fritts, D.C., Tsuda, T., Sato, T., Fukao, S. and Kato, S. (1988) Observational evidence of a saturated gravity wave spectrum in the troposphere and lower stratosphere. J. Atmos. Sci. **45**, 1741–1759.

34) Tsuda, T., Inoue, T., Kato, S., Fukao, S., Fritts, D.C. and VanZandt, T.E. (1989) MST radar observations of a saturated gravity wave spectrum. J. Atmos. Sci. **46**, 2440–2447.

35) VanZandt, T.E. (1985) A model for gravity wave spectra observed by Doppler sounding system. Radio Sci. **20**, 1323–1330.

36) Smith, S.A., Fritts, D.C. and VanZandt, T.E. (1987) Evidence of a saturation spectrum of atmospheric waves. J. Atmos. Sci. **44**, 1404–1410.

37) Dewan, E.M. and Good, R.E. (1986) Saturation and the "universal" spectrum for vertical profiles of horizontal scalar winds in atmosphere. J. Geophys. Res. **91**, 2742–2748.

38) Geller, M.A. (1983) Dynamics of the middle atmosphere. Space Sci. Rev. **34**, 359–375.

39) Tsuda, T., VanZandt, T.E., Mizumoto, M., Kato, S. and Fukao, S. (1991) Spectral analysis of temperature and Brunt-Väisälä frequency fluctuations observed by radiosondes. J. Geophys. Res. **96**, 17265–17278.

40) Kursinski, E.R., Haji, G.A., Schofield, J.T., Linfield, R.P. and Hardy, K.R. (1987) Observing Earth's atmosphere with radio occultation measurements using the Global Positioning System. J. Geophys. Res. **102**, 23429–23465.

41) Anthes, R.A., Ector, D., Hunt, D.C., Kuo, Y.-H., Rocken, C., Schreiner, W.S., Sokolovskiy, S.V., Syndergaard, S., Wee, T.-K., Zeng, Z., Bernhardt, P.A., Dymond, K.F., Chen, Y., Liu, H., Manning, K., Randel, W.J., Trenberth, K.E., Cucurull, L., Healy, S.B., Ho, S.-P., McCormick, C., Meehan, T.K., Thompson, D.C. and Yen, N.L. (2008) The COSMIC/FORMOSAT-3 mission: Early results. Bull. Am. Meteorol. Soc. **89**, 313–333, doi:10.1175/BAMS-89-3-313.

42) Alexander, S.P., Tsuda, T. and Kawatani, Y. (2008) COSMIC GPS Observations of northern hemisphere winter stratospheric gravity waves and comparisons with an atmospheric general circulation model. Geophys. Res. Lett. **35**, L10808, doi:10.1029/2008GL033174.

43) Murayama, Y., Tsuda, T. and Fukao, S. (1994) Seasonal variation of gravity wave activity in the lower atmosphere observed with the MU radar. J. Geophys. Res. **99**, 23057–23069.

44) Alexander, S.P., Klekociuk, A.R. and Tsuda, T. (2009) Gravity wave and orographic wave activity observed around the Antarctic and Arctic stratospheric vortices by the COSMIC GPS-RO satellite constellation. J. Geophys. Res. **114**, doi:10.1029/2009JD011851.

45) Fukao, S. (2006) Coupling Processes in the Equatorial Atmosphere (CPEA): A project overview. J. Meteorol. Soc. Jpn. **84A**, 1–18.

46) McFarlane, N.A. (1987) The effect of orographically excited gravity wave drag on the general circulation of the lower stratosphere and troposphere. J. Atmos. Sci. **44**, 1775–1800.

Profile

Toshitaka Tsuda was born in 1952. After graduating from the Faculty of Engineering at Kyoto University, he started his research career in 1977 with studies on the middle atmosphere dynamics, using radar observations at Kyoto University. He was involved in the design and implementation of the middle and upper atmosphere (MU) radar in Shigaraki, Japan, in 1984, and the equatorial atmosphere radar (EAR) in west Sumatra, Indonesia, in 2001. Since then, he has utilized these radars for studies of atmospheric waves in the middle atmosphere, including atmospheric tides, planetary waves and atmospheric gravity waves. He has also performed pioneering work on the global positioning system (GPS) for observations of atmospheric gravity waves. His research has resulted in extensive subsequent studies demonstrating the utility of GPS for meteorology, atmospheric science and ionosphere physics. He was promoted to Professor at Kyoto University in 1995, and has educated many students in the field of radio and optical remote sensing of the atmosphere. In 2010, he became the Director of the Research Institute for Sustainable Humanosphere (RISH) at Kyoto University. He was elected the president of Japan Geoscience Union (JpGU) in 2012.